muon $g-2$ and the B-physics anomalies in RPV supersymmetry and the discovery prospect at LHC and future colliders

Fang Xu

Collaborators: Bhupal Dev, Amarjit Soni

PPC 2021

Washington University in St. Louis

May 20, 2021

Motivation

- The recent experimental results of muon $g-2$ (from the Fermilab) and the lepton flavor universality violation in rare B-meson decays could be the hints of new physics beyond the Standard Model.
- Under the minimal RPV supersymmetric framework, assuming the mass of third generation sfermions lighter than the other two generations (called "RPV3", proposed in PhysRevD.96.095010 (2017) Altmannshofer, Bhupal Dev, Soni)
- muon $g-2$ and the B-physics anomalies could be addressed simultaneously and also could be detected at LHC and beyond.

muon $g-2$ anomaly

- $\Delta a_\mu = a_\mu^{\rm exp} - a_\mu^{\rm SM} = (251 \pm 59) \times 10^{-11}$ has a significance of 4.2σ.
- Could be the signal of new physics beyond the SM where some new couplings to muon could be detectable by LHC or future colliders.

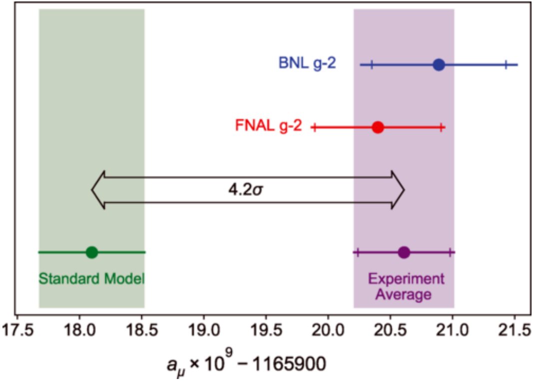

B. Abi et al. PhysRevLett.126.141801 (2021)

B-physics anomalies

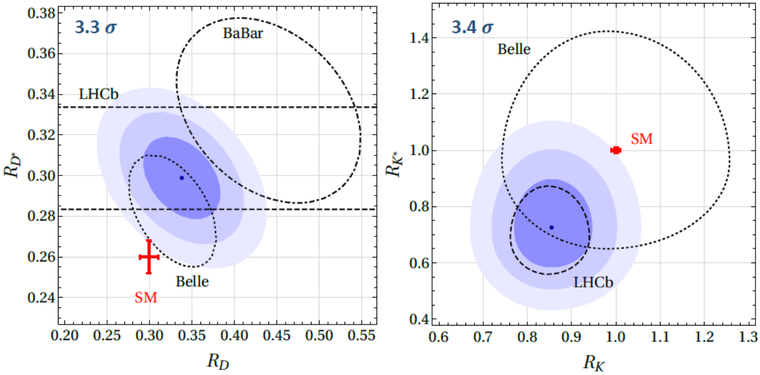

Altmannshofer, Bhupal Dev, Soni, Sui PhysRevD.102.015031

- $R_{D^{(*)}} = \frac{\mathrm{BR}(B \to D^{(*)}\tau\nu)}{\mathrm{BR}(B \to D^{(*)}\ell\nu)}$ (with $\ell = e, \mu$), $R_{K^{(*)}} = \frac{\mathrm{BR}(B \to K^{(*)}\mu^+\mu^-)}{\mathrm{BR}(B \to K^{(*)}e^+e^-)}$
- Also imply the possible new couplings to leptons.

Explanation of anomalies in RPV3 SUSY

- The LQD and LLE part of the RPV SUSY Lagrangian which contains the λ' and λ couplings respectively and are relevant for the $R_{D^{(*)}}$, $R_{K^{(*)}}$ and $(g-2)_\mu$ anomalies.

$$\mathcal{L}_{LQD} = \lambda'_{ijk}(\widetilde{\nu}_{i\mathrm{L}}\overline{d}_{k\mathrm{R}}d_{j\mathrm{L}} + \widetilde{d}_{j\mathrm{L}}\overline{d}_{k\mathrm{R}}\nu_{i\mathrm{L}} + \widetilde{d}^*_{k\mathrm{R}}\overline{\nu}^c_{i\mathrm{L}}d_{j\mathrm{L}} - \widetilde{e}_{i\mathrm{L}}\overline{d}_{k\mathrm{R}}u_{j\mathrm{L}} - \widetilde{u}_{j\mathrm{L}}\overline{d}_{k\mathrm{R}}e_{i\mathrm{L}} - \widetilde{d}^*_{k\mathrm{R}}\overline{e}^c_{i\mathrm{L}}u_{j\mathrm{L}}) + \mathrm{H.c.} \quad (1)$$

$$\mathcal{L}_{LLE} = \frac{1}{2}\lambda_{ijk}\left[\widetilde{\nu}_{i\mathrm{L}}\overline{e}_{k\mathrm{R}}e_{j\mathrm{L}} + \widetilde{e}_{j\mathrm{L}}\overline{e}_{k\mathrm{R}}\nu_{i\mathrm{L}} + \widetilde{e}^*_{k\mathrm{R}}\overline{\nu}^c_{i\mathrm{L}}e_{j\mathrm{L}} - (i \leftrightarrow j)\right] + \mathrm{H.c.} \quad (2)$$

- Following the discussions in PhysRevD.102.015031 Altmannshofer, Bhupal Dev, Soni, Sui, in RPV3 framework, $(g-2)_\mu$ correction can be written as:

$$\Delta a_\mu = \frac{m_\mu^2}{96\pi^2}\sum_{k=1}^{3}\left(\frac{2(|\lambda_{32k}|^2 + |\lambda_{3k2}|^2)}{m^2_{\widetilde{\nu}_\tau}} - \frac{|\lambda_{3k2}|^2}{m^2_{\widetilde{\tau}_\mathrm{L}}} - \frac{|\lambda_{k23}|^2}{m^2_{\widetilde{\tau}_\mathrm{R}}} + \frac{3|\lambda'_{2k3}|^2}{m^2_{\widetilde{b}_\mathrm{R}}}\right) \quad (3)$$

Explanation of anomalies in RPV3 SUSY

$(g-2)_\mu$

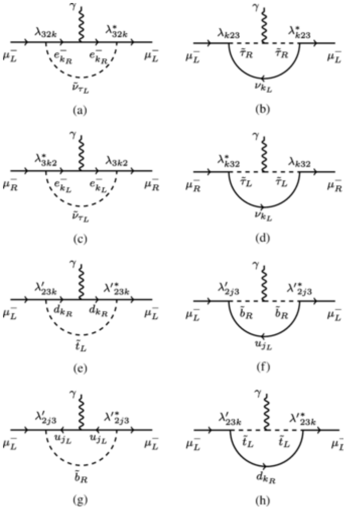

$R_{D^{(*)}}$

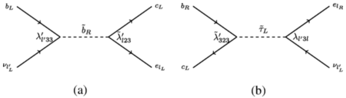

$R_{K^{(*)}}$

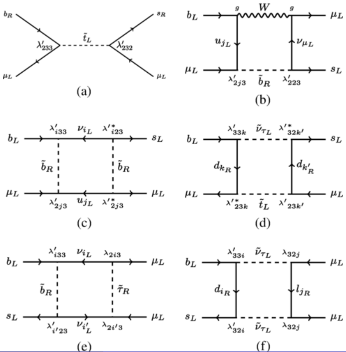

Parameters and benchmark scenario

- Parameters $(\lambda_{232}, \lambda'_{233}, \lambda'_{223}, \lambda'_{232}, m_{\tilde{b}_R}, m_{\tilde{b}_L}, m_{\tilde{\nu}_\tau}, m_{\tilde{\tau}_L})$
  - $\lambda_{232} = -\lambda_{322} \neq 0 \Leftarrow$ contribute to muon $g-2$, other λ_{3ij} couplings cannot be large at the same time due to the constraints of $\tau \to \mu\mu\mu$, $\tau \to e\mu\mu$ etc.
  - $\lambda'_{2ij} \neq 0 \Leftarrow$ include μ and free of $m_{\tilde{\nu}_\tau}$, otherwise, λ'_{3ij} combined with λ_{32k} or λ_{3k2}, well measured meson decays $(\bar{d}_i d_j) \to \mu\ell_k$ or $\tau \to \mu K$ and $\tau \to \mu\eta$ decays will prevent λ'_{3ij} to be large.
  - $m_{\tilde{\tau}_R}$ not involved with this choice of couplings.
  - $m_{\tilde{t}_L}$ can only influence $\mathrm{BR}(B_s \to \mu^+\mu^-)$ and the Wilson coefficients $(C'_9)^\mu$ and $(C'_{10})^\mu$ that describe the $R_{K^{(*)}}$ anomaly. But we can assume a relatively larger value to eliminate the influence and it is not considered as a parameter.

Parameters and benchmark scenario

- Furthermore, assume $(\lambda_{232}, \lambda'_{233} = -\lambda'_{223} = -3\lambda'_{232}, m_{\tilde{b}_R} = m_{\tilde{b}_L}, m_{\tilde{\nu}_\tau}, m_{\tilde{\tau}_L} = 4\text{TeV})$ then we can plot the anomalies and constraints in the two-dimensional parameter space: $(\lambda'_{233}, m_{\tilde{b}_R})$ and $(\lambda_{232}, m_{\tilde{\nu}_\tau})$
  - $m_{\tilde{b}_R} = m_{\tilde{b}_L}$ for simplicity.
  - $m_{\tilde{\tau}_L}$ has opposite contribution for $(g-2)_\mu$. The influence is not important as long as $m_{\tilde{\tau}_L} \gtrsim O(1\text{TeV})$. Here we choose 4 TeV.
  - $\lambda'_{233} = -\lambda'_{223} \Leftarrow \lambda'_{233}$, λ'_{223} and $m_{\tilde{b}_R}$ are the only parameters that influence $R_{D^{(*)}}$ and $R_{K^{(*)}}$ in our scenario. Assuming $\lambda'_{233} = \epsilon_1 \lambda'_{223}$, we found that $\epsilon_1 \sim (-3, -1)$ will give an overlap region of $R_{D^{(*)}}$ and $R_{K^{(*)}}$. When $|\epsilon_1|$ decrease, the coupling λ'_{233} of the overlap region will also decrease, so we choose $\epsilon_1 = -1$ here.
  - $\lambda'_{233} = -\lambda'_{223} = -3\lambda'_{232} \Leftarrow \lambda'_{233}$, λ'_{223}, λ'_{232}, $m_{\tilde{b}_R}$ and $m_{\tilde{b}_L}$ are relevant for the constraints of $B \to K\nu\overline{\nu}$, $B_s - \overline{B}_s$ mixing and $D^0 \to \mu^+\mu^-$. Assuming $\lambda'_{233} \approx -\lambda'_{223} = \epsilon_2 \lambda'_{232}$, we found that $\epsilon_2 \sim (-6, -2)$, where $\epsilon_2 = -3$ gives the best fit.

Simulations

- Consider the processes $pp \to \bar{t}\mu^+\mu^-$ ($pp \to t\mu^+\mu^-$ is similar but with a larger background cross-section)
- Background:

Table 1: $pp \to \bar{t}\mu^+\mu^- X$ cross sections (fb)

X	14 TeV	$M_{\mu^+\mu^-} > 0.15$ TeV	27 TeV	$M_{\mu^+\mu^-} > 0.15$ TeV	100 TeV	$M_{\mu^+\mu^-} > 0.15$ TeV
j	0.381	3.35×10^{-3}	1.06	1.05×10^{-2}	5.83	7.11×10^{-2}
b	4.23×10^{-3}	3.64×10^{-5}	9.47×10^{-3}	9.85×10^{-5}	3.84×10^{-2}	3.92×10^{-4}
$W^+ \to jj$	3.76×10^{-3}	2.75×10^{-5}	1.49×10^{-2}	1.33×10^{-4}	0.133	1.58×10^{-3}
$W^+ \to e^+\nu_e$	6.38×10^{-4}	5.68×10^{-6}	2.53×10^{-3}	2.68×10^{-5}	2.24×10^{-2}	2.28×10^{-4}
$W^+ \to \mu^+\nu_\mu$	6.15×10^{-3}	2.67×10^{-3}	2.64×10^{-2}	1.12×10^{-2}	0.242	0.120
$W^+ \to \tau^+\nu_\tau$	6.34×10^{-4}	6.09×10^{-6}	2.52×10^{-3}	3.08×10^{-5}	2.25×10^{-2}	2.81×10^{-4}
Total	0.396	6.10×10^{-3}	1.12	2.20×10^{-2}	6.29	0.194

[a] $p_T^{j,b,l} < 20$ GeV, $E_T^{\rm miss} < 20$ GeV
[b] $p_T^{t,\mu} > 20$ GeV, $|\eta^{t,\mu}| < 2.5$

Simulations

- Signal:

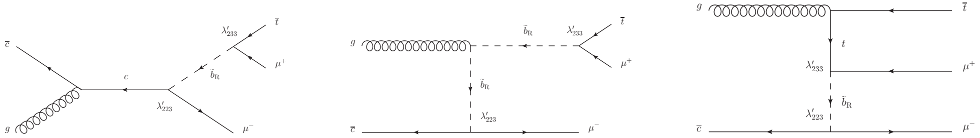

(a) (b) (c)

- Only λ'_{233}, λ'_{223} and $m_{\tilde{b}_\text{R}}$ contribute to the process $pp \to \bar{t}\mu^+\mu^-$. And what can be probed are actually these parameters, a projection of the scenario.
- Assume the luminosity $\mathscr{L} = 3000\ \text{fb}^{-1}$. $\sqrt{s} = 14\ \text{TeV}, 27\ \text{TeV}, 100\ \text{TeV}$.
- Signal significance $N = \frac{S}{\sqrt{S+B}}$.

Invariant mass distribution

- Invariant mass $M_{\mu^+\mu^-}$ distributions at $\sqrt{s} = 14\ \mathrm{TeV}, 27\ \mathrm{TeV}, 100\ \mathrm{TeV}$

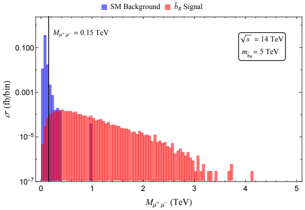

(d)

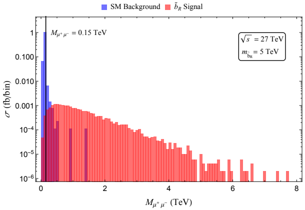

(e)

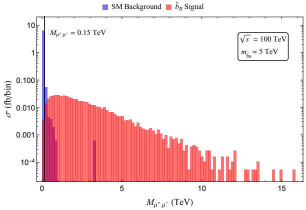

(f)

- We have used $\lambda'_{233} = -\lambda'_{223} = 1.3$, $m_{\tilde{b}_R} = 5\ \mathrm{TeV}$ for the signal process.
- $p_T^{t,\mu} > 20$ GeV, $|\ \eta^{t,\mu}\ | < 2.5$, $\Delta R^{\mu\mu} > 0.4$ and $\Delta R^{t\mu} > 0.4$ for the minimal trigger cuts of $\bar{t}\mu^+\mu^-$

Anomalies and constraints in the parameter space

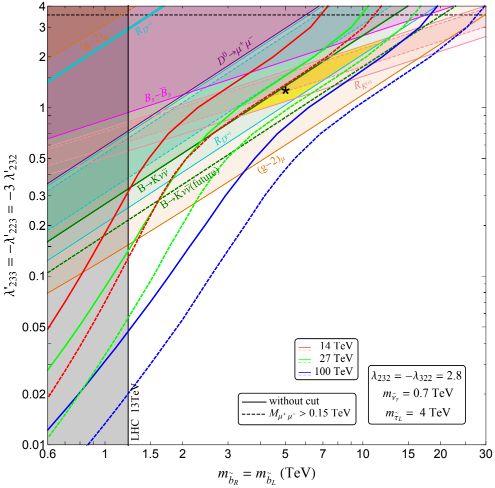

(g)

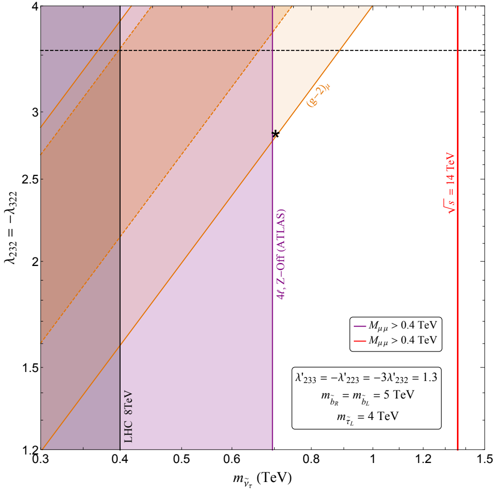

(h)

Anomalies and constraints in the parameter space

- The figure on the left corresponds to the black star in the figure on the right and vice versa.
- The invariant mass distributions are calculated at the value of black star in the figure on the left.
- Since many anomalies and constraints are independent of $(\lambda_{232}, m_{\tilde{\nu}_\tau})$, they become just numbers instead of curves in the figure on the right.

Anomaly/Constraint	Quantities in Figure(h)	Experimental value/limit
$R_{D^{(*)}}$	$\frac{R_{D^{(*)}}}{R^{\rm SM}_{D^{(*)}}} = 1.05$	1.15 ± 0.04
$R_{K^{(*)}}$	$(C_9)^\mu = -(C_{10})^\mu = -0.23$	-0.35 ± 0.08
$D^0 \to \mu^+\mu^-$	${\rm BR}(D^0 \to \mu^+\mu^-) = 2.8 \times 10^{-10}$	$< 7.6 \times 10^{-9}$ (95% CL)
$B \to K^{(*)}\nu\bar{\nu}$	$R_{B\to K^{(*)}\nu\bar{\nu}} = \frac{{\rm BR}(B\to K^{(*)}\nu\bar{\nu})}{{\rm BR}_{\rm SM}(B\to K^{(*)}\nu\bar{\nu})} = 4.6$	< 5.2 (95% CL)
$B_s - \overline{B}_s$ mixing	$\Delta M_{B_s} = (20.12 \pm 1.7)\ {\rm ps}^{-1}$	$(17.757 \pm 0.021)\ {\rm ps}^{-1}$

Discussions

- The red, green and blue lines are the signal significance $N = 2$ curves at the center of mass energy $\sqrt{s} = 14$ TeV, 27 TeV and 100 TeV separately, before (solid lines) and after (dashed lines) applying the cut $M_{\mu^+\mu^-} > 0.15$ TeV.
- All the region above these curves corresponds to the signal significance $N > 2$. These curves bend downward because of the off-shell contribution of $pp \to \bar{t}\mu^+\mu^-$
- The yellow shaded region is the overlap of $(g-2)_\mu$, $R_{D^{(*)}}$ and $R_{K^{(*)}}$ favored region at 3σ level.
- This region is detectable when $\sqrt{s} > 27\ \mathrm{TeV}$ at signal significance $N = 2$ level. It is the best scenario we can find for the detection purpose. Changing the value of $|\epsilon_1|$ could move the yellow shaded region to the upper left direction, but the detection curves will also move to the left faster than the yellow shaded region.
- We also put a future $B \to K^{(*)}\nu\bar{\nu}$ constraint line $(R_{B\to K^{(*)}\nu\bar{\nu}} = 1)$ that can exclude the yellow shaded region.

Discussions

- $m_{\widetilde{b}_\mathrm{R}} \sim 3 - 12$ TeV, $m_{\widetilde{\nu}_\tau} \sim 0.7 - 0.9$ TeV $\Rightarrow$ The first term in Eq(3) gives the main contribution of Δa_μ. The third term cannot be large due to the constraint of $B \to K^{(*)}\nu\overline{\nu}$ as one can see from Fig(g).
- The lower bound of $m_{\widetilde{\nu}_\tau}$ comes from the 4-lepton search of ATLAS (ATLAS-CONF-2021-011). The 4-lepton signal in our scenario comes from the pair production of $\widetilde{\nu}_\tau$ (+ jet) with $\widetilde{\nu}_\tau \to \mu^+\mu^-$, and we have also used the cut $M_{\mu\mu} > 0.4$ TeV.
- The red solid line in the figure on the right corresponds to the signal significance $N = 2$ when the $\sqrt{s} = 14$ TeV.
- The whole $(g-2)_\mu$ favored region is detectable at 14 TeV although we cannot see the information of couplings.